ChemComm

COMMUNICATION

View Article Online
View Journal | View Issue

Cite this: *Chem. Commun.*, 2014, **50**, 3238

Received 27th January 2014,
Accepted 5th February 2014

DOI: 10.1039/c4cc00700j

www.rsc.org/chemcomm

Does functionalisation enhance CO_2 uptake in interpenetrated MOFs? An examination of the IRMOF-9 series†

Ravichandar Babarao,*[a] Campbell J. Coghlan,[b] Damien Rankine,[b] Witold M. Bloch,[b] Gemma K. Gransbury,[b] Hiroshi Sato,[c] Susumu Kitagawa,[c] Christopher J. Sumby,[b] Matthew R. Hill*[a] and Christian J. Doonan*[b]

The effect of pore functionalisation (–I, –OH, –OCH_3) on a series of topologically equivalent, interpenetrated metal–organic frameworks (MOFs) was assessed by both simulation and experiment. Counter-intuitively, a decreased affinity for CO_2 was observed in the functionalised materials, compared to the non-functionalised material. This result highlights the importance of considering the combined effects of network topology and chemical functionality in the design of MOFs for enhanced CO_2 adsorption.

Capturing CO_2 from major anthropogenic sources such as coal-fired power plants is an area of intense research. One of the main challenges for chemists is the development of novel energy-efficient gas separation processes. Several strategies have been proposed including physical adsorption,[1] absorption by solvents,[2] and gas separation membranes.[3–5] Indeed, recent work has shown that physical adsorption of CO_2 in MOFs is a promising low-energy alternative to conventional methods.[1] A commonly employed strategy to enhance CO_2 adsorption capacity at low pressures in MOFs is to incorporate moieties that have a high affinity for CO_2. As a result, such materials give rise to significant enthalpies of adsorption.[2,3] In addition to tailoring the functionality of the framework, careful control over the internal pore size is important as a there is a trade-off between maximising the potential energy well overlap between the pore walls at close distances, and loss of available pore volume.[4] For example, although framework interpenetration reduces the gravimetric gas uptake of a given material it has been shown to assist CO_2 uptake, highlighting the importance of tailoring both functionality and pore confinement.[5] In the case mentioned, the unusual and enhanced CO_2 adsorption shown by the framework is linked to the stepwise filling of pores and structural vacancies.

Modelling and experimental studies have shown that pore functionalisation generally improves the CO_2 uptake in non-interpenetrated frameworks.[2,6–13] However, we note that the effect of functional groups on CO_2 capacity in interpenetrated MOFs is not well documented.[14] A recent study showed that combining both interpenetration and functionality in a MOF can enhance both H_2 and CO_2 uptake, taking advantage of their individual effects.[15] Here however, we show, for interpenetrated $[Zn_4O(BPDC)_3]$ IRMOF derivatives (Scheme 1), that these effects do not necessarily combine to enhance CO_2 uptake. Accordingly, careful consideration of both the framework architecture and functionality is required for the development of suitable physisorbents for CO_2 capture and separation.

We previously demonstrated that by carefully controlling reaction conditions, phase-pure isostructural MOFs with interpenetrated and non-interpenetrated structures can be synthesised.[16] Here we expand this study by investigating a series of, topologically analogous, interpenetrated MOFs constructed from functionalised biphenyl links (Scheme 1) with the aim of understanding the impact of functional groups on CO_2 uptake.[16] Notably, our results show that irrespective of the functional group, a decrease in CO_2 uptake is observed when compared to that of the non-functionalised material, IRMOF-9. This is quite surprising given that functionalisation in non-interpenetrated frameworks is generally observed to enhance CO_2 affinity. Here we use molecular modelling to shed light on how functional groups block the inaccessible regions (*i.e.* small pores) present in functionalised IRMOF-9 analogues (Fig. 1). This highlights that the increased potential-well overlap due to

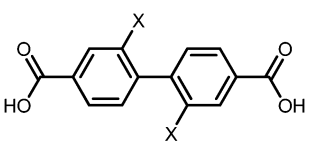

X = H, OH, OCH_3, I

Scheme 1

[a] *CSIRO Division of Materials Science and Engineering, Clayton South MDC, VIC3169, Australia. E-mail: matthew.hill@csiro.au, ravichandar.babarao@csiro.au; Fax: +61 3 9545 2837; Tel: +61 3 9545 2943*

[b] *School of Chemistry & Physics, The University of Adelaide, Adelaide, Australia. E-mail: christian.doonan@adelaide.edu.au; Fax: +61 8 8313 4358; Tel: +61 8 8303 5770, +61 8 8313 7406*

[c] *Institute for Integrated Cell-Material Sciences, Kyoto University, Japan*

† Electronic supplementary information (ESI) available: Experimental and simulation details and additional results. See DOI: 10.1039/c4cc00700j

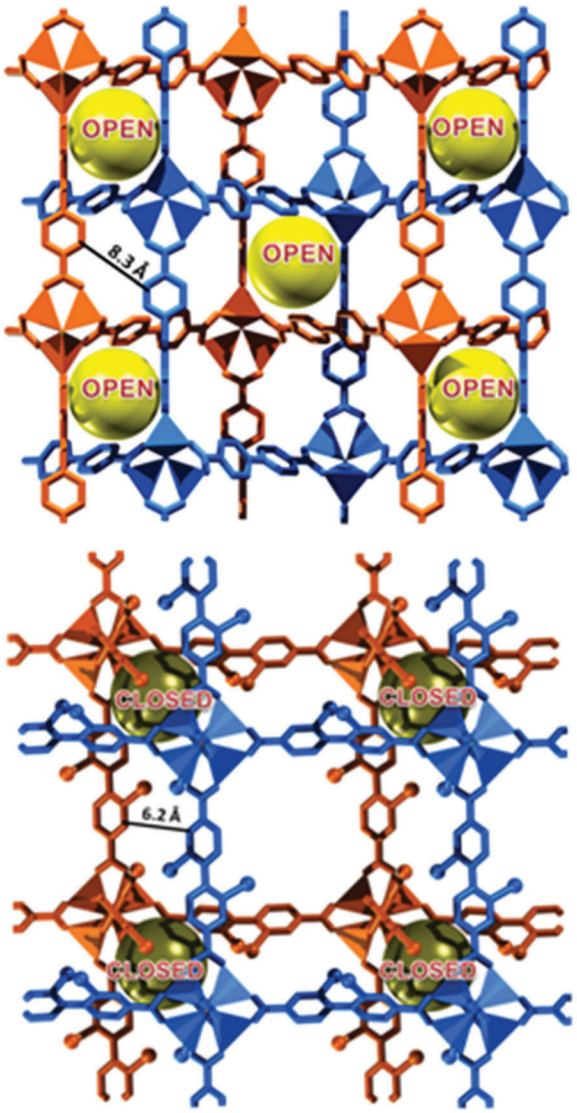

Fig. 1 Schematic representation of IRMOF-9 (top) and iodo functionalised IRMOF-9 (bottom), with inter-framework distances of 8.3 and 6.2 Å respectively, showing accessible (yellow ball) and inaccessible (dark green ball) small pores for gas uptake.

small pores is more important energetically than the presence of functional groups in enhancing CO_2 uptake, particularly at low pressure.[17–19]

IRMOF-9 [$Zn_4O(BPDC)_3$] and its functionalised analogues (–OH, $–OCH_3$) were prepared as reported in previous work.[16] Iodo functionalised IRMOF-9 (IRMOF-9–I) was synthesised using a slightly modified method (see ESI†). The functionalised IRMOF-9 materials are an isostructural series consisting of Zn_4O tetrahedral clusters acting as six-connecting nodes with the functional groups directed into the smaller pores that are formed by interpenetration.[16] CO_2 and N_2 gas isotherms were measured for each MOF (Table 1 and Fig. 2) and Grand Canonical Monte Carlo (GCMC) simulations were employed to predict pure CO_2 isotherms and NVT simulation to predict the heat of adsorption at infinite loading (see ESI†).

BET analysis of the 77 K N_2 isotherm for each MOF showed a reduction in surface area for the functionalised materials.

Table 1 Framework density, pore volumes, accessible volumetric surface area and isosteric heat of adsorption at low coverage predicted from NVT simulation with blocking of the inaccessible pore regions (except for IRMOF-9)

Structure	ρ_f (g cm^{-3})	V_{free} (cm^3 g^{-1})	Volumetric surface area (m^2 cm^{-3})	Q_{st}^0 CO_2 (kJ mol^{-1})
IRMOF-9	0.636	1.18	1918	22.73
IRMOF-9–OH	0.705	0.99	1619(1262)[a]	16.95
IRMOF-9–OCH_3	0.773	0.84	1573(1317)[a]	18.55
IRMOF-9–I	0.878	0.76	1730(1184)[a]	15.94

[a] Experimental BET surface area based on N_2 isotherms.

This observation is in qualitative agreement with the predicted surface area based on nitrogen as a probe molecule (Table 1). Excepting IRMOF-9, typical type I isotherms were observed for all the functionalised analogues. Due to weak inter-framework interactions in IRMOF-9 (Fig. 1), evidence of gating behaviour was observed in the N_2 as well as CO_2 isotherms at 195 K (Fig. S3 and S4, ESI†). Such gating behaviour has been found recently in a two-fold interpenetrated framework and also in a partially interpenetrated framework.[5,20] In the present case, structural transformations occur under pressure for CO_2 showing multiple steps at 195 K. It is noteworthy that this is the first time such an adsorption profile has been reported for IRMOF-9. We attribute this to careful handling and activation procedures (see ESI†). Addition of functional groups to the IRMOF-9 backbone enhances the inter-framework interactions (Fig. 1) and eliminates adsorption gating behaviour. Similar behaviour has been observed in many interpenetrated MOFs with pendant groups attached to the BPDC linkers.[21–23] The type I isotherms suggest that functionalised IRMOF-9 derivatives, behave more like a rigid open framework due to a lack of dynamic motion.

Next, we investigated the CO_2 gas adsorption in IRMOF-9 and its functionalised analogues at room temperature (Fig. 2). No adsorption–desorption hysteresis was observed for either IRMOF-9 or the functionalised frameworks at temperatures

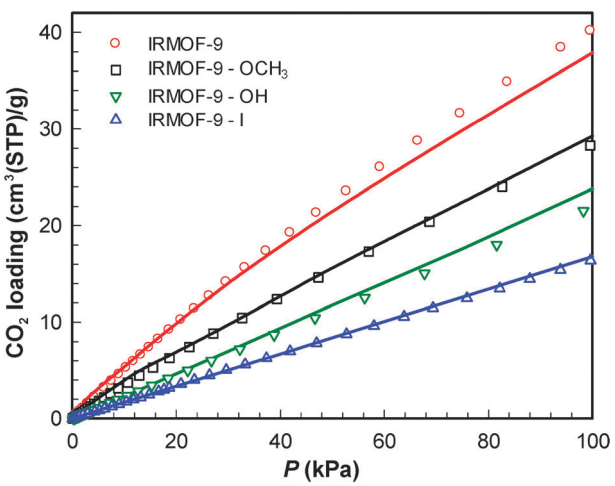

Fig. 2 CO_2 uptake in interpenetrated IRMOF-9 and functionalised IRMOF-9 frameworks at 298 K. Simulations show that blocking the inaccessible pore in the functionalised IRMOF-9 materials provides excellent agreement to experiment. The empty symbols represent experimental data, while the solid lines represent simulated data.

above the triple point. Fig. 2 shows good agreement between the simulated data and the experimental values for IRMOF-9 and the functionalised materials, when the inaccessible region is blocked in the simulation (see Fig. S11 and S12, ESI†). The experimental CO_2 uptake of IRMOF-9 was measured to be 40 $cm^3\ g^{-1}$ at 100 kPa and was found to decrease drastically to 28 $cm^3\ g^{-1}$ in IRMOF-9–OCH_3 and to 16 $cm^3\ g^{-1}$ in IRMOF-9–I, respectively.

This observation can be rationalised from an energetic viewpoint as the calculated adsorption enthalpy at low coverage from NVT simulations and dispersion corrected density functional theory is highest in IRMOF-9, followed by –OCH_3, –OH and –I frameworks (Table 1 and Table S7, ESI†). As amino groups are widely employed for enhancing CO_2 uptake, we further predicted CO_2 uptake using GCMC simulation and found the CO_2 capacity in IRMOF-9–NH_2 is lower than that of IRMOF-9 (see Fig. S13, ESI†). We posit that the decrease in CO_2 uptake observed for the functionalised IRMOF-9 frameworks can be attributed to the blockage of small pores by the attached functional group and presence of pores with larger diameters.

Fig. 3 shows the pore size distribution obtained from the N_2 isotherm data of IRMOF-9 and its functionalised forms. As shown in Fig. 3 the pore sizes present in IRMOF-9 are centred around 5.8 Å and 8.0 Å (larger pores not shown in Fig. 3), however, for the functionalised analogues only one distinct pore is present centred at 11 or 12 Å. Presumably, this is because the pendant functional groups enhance the Van der Waal's and electrostatic interactions between the frameworks creating a more uniform pore size. To examine the location of CO_2 in the IRMOFs, density contours of CO_2 obtained from GCMC simulations were prepared (Fig. S14, ESI†). In IRMOF-9, the CO_2 is exclusively located in the small pores created by the interpenetration of frameworks where the effective potential energy well-overlap occurs between metal clusters and phenyl linkers. However, in the functionalised IRMOF-9 forms, the CO_2 is mainly located in the larger pores in close proximity to the functional group, as the equivalent small cavities are inaccessible for gas molecules, even for H_2 (see Fig. S15, ESI†).

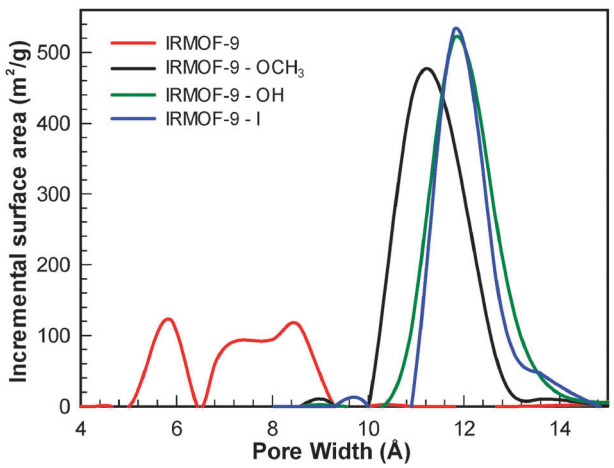

Fig. 3 Pore size distributions based on N_2 isotherms showing different pore sizes in IRMOF-9, but only one distinct pore in functionalised IRMOF-9 frameworks.

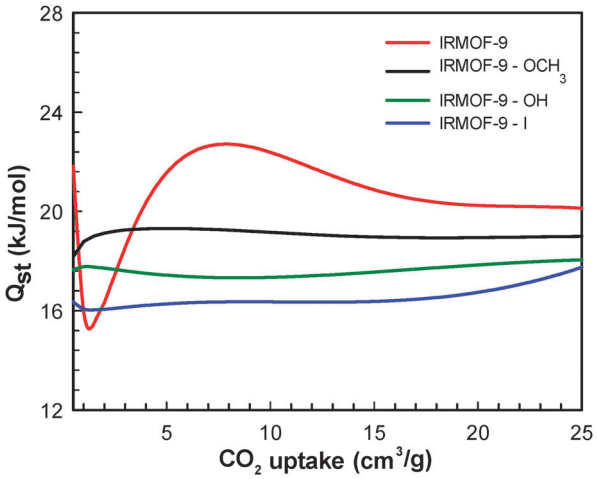

Fig. 4 Isosteric heat of adsorption as a function of simulated CO_2 uptake using Clausius–Clapeyron equation.

In addition, the binding energy of one CO_2 molecule from first principles DFT calculations displayed a similar behaviour implying that the CO_2 uptake correlates well with the CO_2-functional group interactions (Fig. S16 and Table S7, ESI†).

Fig. 4 shows the predicted isosteric heat of adsorption from the Clausius–Clapeyron equation based on simulated adsorption isotherms at 273 K and 298 K. Consistent with CO_2 adsorption capacity shown in Fig. 2, the heat of adsorption decreases in the order IRMOF-9–OCH_3 > –OH > –I. The key result in this instance is that the increased relevance of small pores in IRMOF-9 supersedes the chemical attraction of functional groups in the derivatised analogues, as these groups are largely occluded within the interpenetrated structure. Secondly, in IRMOF-9, variations of enthalpy strength at low loading are observed. The initial decrease in isosteric heat may attributed to the multiple pore sizes present in IRMOF-9[25] (Fig. 3) in which the more energetically favourable and smaller pores are occupied first followed by the less favourable sites as loading increases. As the gas loading is increased, the co-operative interaction between CO_2 molecules is enhanced resulting in a larger isosteric heat of adsorption. A similar trend has been observed earlier for CO_2 adsorption in C_{168} and N_2 and CO in $AlPO_4$-5 structures and CO_2 in an interpenetrated MOF.[24,25] However, we also modelled the heat of adsorption for IRMOF-9 using virial equation methods (Fig. S17, ESI†). Using this approach the initial enthalpy of adsorption is, also, approximately 22 kJ mol^{-1} and decreases slightly over the coverage range. However, the dip at low pressure is absent.

In conclusion, we have shown that the general strategies for enhancement of CO_2 uptake, particularly functionalising linkers in non-interpenetrated MOFs do not translate to interpenetrated analogues. The smaller pore size in these species is the dominant factor in the control of CO_2 adsorption capacities. This is because functionalisation increases the inter-framework interactions and in turn blocks the small pores, a critical factor for enhancing CO_2 uptake at low partial pressures. Molecular simulation showed a similar trend in CO_2 uptake, which agrees well with the experimental data, when the inaccessible pore region of the functionalised

frameworks was blocked. The smaller pores in IRMOF-9 enhance the CO_2 isosteric heat Q_{st}^0, and consequently, increase CO_2 uptake. In general, to make use of the small pores created in interpenetrated frameworks utilising a simple linker without any functional groups might be a good choice for enhancing CO_2 uptake, particularly at low pressure.

This research is supported by the Science and Industry Endowment Fund (SIEF). CJD and CJS would like to acknowledge the Australian Research Council for funding FT100100400 and FT0991910, respectively.

Notes and references

1 P. Nugent, Y. Belmabkhout, S. D. Burd, A. J. Cairns, R. Luebke, K. Forrest, T. Pham, S. Ma, B. Space, L. Wojtas, M. Eddaoudi and M. J. Zaworotko, *Nature*, 2013, **495**, 80.
2 T. M. McDonald, D. M. D'Alessandro, R. Krishna and J. R. Long, *Chem. Sci.*, 2011, **2**, 2022.
3 T. M. McDonald, W. R. Lee, J. A. Mason, B. M. Wiers, C. S. Hong and J. R. Long, *J. Am. Chem. Soc.*, 2012, **134**, 7056.
4 A. W. Thornton, D. Dubbeldam, M. S. Liu, B. P. Ladewig, A. J. Hill and M. R. Hill, *Energy Environ. Sci.*, 2012, **5**, 7637.
5 S. Yang, X. Lin, W. Lewis, M. Suyetin, E. Bichoutskaia, J. E. Parker, C. C. Tang, D. R. Allan, P. J. Rizkallah, P. Hubberstey, N. R. Champness, K. M. Thomas, A. J. Blake and M. Schroeder, *Nat. Mater.*, 2012, **11**, 710.
6 R. Babarao, S. Dai and D. Jiang, *Langmuir*, 2011, **27**, 3451.
7 S. Biswas and P. Van der Voort, *Eur. J. Inorg. Chem.*, 2013, 2154.
8 A. Das, M. Choucair, P. D. Southon, J. A. Mason, M. Zhao, C. J. Kepert, A. T. Harris and D. M. D'Alessandro, *Microporous Mesoporous Mater.*, 2013, **174**, 74.
9 A. Demessence, D. M. D'Alessandro, M. L. Foo and J. R. Long, *J. Am. Chem. Soc.*, 2009, **131**, 8784.
10 W. Mu, D. Liu, Q. Yang and C. Zhong, *Microporous Mesoporous Mater.*, 2010, **130**, 76.
11 N. Planas, A. L. Dzubak, R. Poloni, L.-C. Lin, A. McManus, T. M. McDonald, J. B. Neaton, J. R. Long, B. Smit and L. Gagliardi, *J. Am. Chem. Soc.*, 2013, **135**, 7402.
12 D. Wu, Q. Yang, C. Zhong, D. Liu, H. Huang, W. Zhang and G. Maurin, *Langmuir*, 2012, **28**, 12094.
13 S. S. Han, D.-H. Jung and J. Heo, *J. Phys. Chem. C*, 2013, **117**, 71.
14 H.-L. Jiang, T. A. Makal and H.-C. Zhou, *Coord. Chem. Rev.*, 2013, **257**, 2232.
15 P. Pachfule, Y. Chen, J. Jiang and R. Banerjee, *J. Mater. Chem.*, 2011, **21**, 17737.
16 D. Rankine, A. Avellaneda, M. R. Hill, C. J. Doonan and C. J. Sumby, *Chem. Commun.*, 2012, **48**, 10328.
17 N. C. Burtch, H. Jasuja, D. Dubbeldam and K. S. Walton, *J. Am. Chem. Soc.*, 2013, **135**, 7172.
18 L. Liu, K. Konstas, M. R. Hill and S. G. Telfer, *J. Am. Chem. Soc.*, 2013, **135**, 17731.
19 A. Schoedel, W. Boyette, L. Wojtas, M. Eddaoudi and M. J. Zaworotko, *J. Am. Chem. Soc.*, 2013, **135**, 14016.
20 K. L. Mulfort, O. K. Farha, C. D. Malliakas, M. G. Kanatzidis and J. T. Hupp, *Chem.–Eur. J.*, 2010, **16**, 276.
21 A. D. Burrows, C. G. Frost, M. F. Mahon and C. Richardson, *Angew. Chem., Int. Ed.*, 2008, **47**, 8482.
22 A. D. Burrows, C. G. Frost, M. F. Mahon and C. Richardson, *Chem. Commun.*, 2009, 4218.
23 T.-H. Park, K. Koh, A. G. Wong-Foy and A. J. Matzger, *Cryst. Growth Des.*, 2011, **11**, 2059.
24 R. Babarao, Z. Hu, J. Jiang, S. Chempath and S. I. Sandler, *Langmuir*, 2007, **23**, 659.
25 Z. Zhang, S. Xiang, K. Hong, M. C. Das, H. D. Arman, M. Garcia, J. U. Mondal, K. M. Thomas and B. Chen, *Inorg. Chem.*, 2012, **51**, 4947.